Journal of Applied Sciences Research

2018 December; 14(6): pages 11-17
DOI: 10.22587/jasr.2018.14.6.3

Research Article
Homepage:http://www.aensiweb.com/JASR/

AENSI Publications

Degradation of AISI 630 exposed to CO_2-saturated saline aquifer at ambient pressure and 100 bar

Anja Pfennig [1], Axel Kranzmann [2]

[1] HTW University of Applied Sciences Berlin, Wilhelminenhofstraße 75 A, Gebäude C, 12459 Berlin
[2] BAM Federal Institute of Materials Research and Testing, Unter den Eichen 87, 12205 Berlin

Correspondence Author: Anja Pfennig, *HTW University of Applied Sciences Berlin, Wilhelminenhofstraße 75 A, Gebäude C, 12459 Berlin*

Received date: 23 October 2018, Accepted date: 15 November 2018, Online date: 25 December 2018

Abstract

In general high alloyed steels are suitable as pipe steels for carbon capture and storage technology (CCS), because they provide sufficient resistance against the corrosive environment of CO_2-saturated saline aquifer which serves as potential CCS-site in Germany. High alloyed martensitic steel AISI 630 has been proven to be sufficient resistant in corrosive environments, e.g. regarding heat, pressure, salinity of the aquifer, CO_2-partial pressure), but reveals a distinct corrosion pattern in CCS environment. Therefore coupons of AISI 630 heat treated using usual protocols were kept at T=60 °C and ambient pressure as well as p=100 bar up to 8000 h in an a) water saturated supercritical CO_2 and b) CO_2-saturated synthetic aquifer environment similar to on-shore CCS-sites in the Northern German Basin. AISI 630 precipitates a discontinuous ellipsoidal corrosion layer after being exposed for more than 4000 hours. Best corrosion resistance in the CO_2-saturated synthetic aquifer environment phase is achieved via normalizing prior to exposure. In water saturated supercritical CO_2 tempering at medium temperatures after hardening gives lowest corrosion rates. Corrosion fatigue via push-pull tests with a series of 30 specimens was evaluated at stress amplitudes between 150 MPa and 500 MPa (sinusoidal dynamic test loads, R=-1; resonant frequency ~ 30 Hz). The endurance limit of AISI 630 is reduced by more than 50% when exposed to CCS environment (maximum number of cycles (10 x 10^6) at a stress amplitude of 150 MPa).

Key words: Corrosion Fatigue, High Cycle Fatigue, Steel, Ccs, Co2-Storage, Geothermal Energy, In-Situ Experiment

INTRODUCTION

During CCS (Carbon Capture and Storage [1], [2]) emission gasses from combustion processes of power plants are separated, cleaned, transported to and injected directly into deep geological layers [3]- [9]. The corrosion of tubing steels may become a reliability issue because CO_2-corrosion is sensitively dependent on

- alloy composition,
- contamination of alloy and media,
- temperature,
- CO_2 partial pressure,
- protective corrosion scales
- flow conditions [5], [6], [10]-[21].

Alloying elements [22] as well as heat treatment (temperature and time of austenitizing, cooling rate as well as temperature and time of annealing [23],[24],[25]) shows significant influence upon the corrosion resistance of steels, e.g.. high Ni- and Cr contents [26],[27] improve general corrosion resistance as well as retained austenite improves pitting corrosion resistance [26]. Higher austenitizing temperature of martensitic steels [28],[29],[30] as well as higher annealing temperature of lean duplex stainless steels [22], [23], [28] decrease the pitting potential. Due to reactive grain boundaries in martensitic microstructure C-Mn (carbon) steels in a H_2S-containing NaCl solution shows higher corrosion rates than ferritic or ferritic-bainitic microstructures [31].

Corrosion phenomena were also found to be reason for early failure of materials under cyclic load [32],[33],[34]. Pit formation on stainless steels is enhanced by chemical reactions, local changes of lattice energy within the steel`s surface and mechanical load [35],[36]. Higher grain/phase boundary energy where dual or triple points of grain/phase boundaries occur enhances crack initiation and accelerates crack propagation [32],[34]. This local lattice mismatch also initiates pit -, selective - and inter granular corrosion that lead to crack formation [33]. A possible crack initiation model was presented by Han et al. [37] and modified by Pfennig et al. [35], [36], [38] (Fig. 1).

Surface corrosion layers grow slowly and locally corroded samples usually show the same corrosion products as surface layers [15], [17], acting as corrosion catalyser. Generally siderite $FeCO_3$ [3],[38],[39],[40] is formed on steels exposed to CO_2-environment (a) due to the low solubility of $FeCO_3$ in water (p_{Ksp} = 10.54 at 25 °C [29], [37]) leading to anodic iron dissolution. The initial formation of transient $Fe(OH)_2$ [6], [30] (grey area in: a) possibly leads to an increase of the local pH near the hydroxide film. As a consequence an internal and external ferrous carbonate film precipitates, Han et. al [37] (a and b) according to equations 1 to 6 [15], [29]:

Citation: Anja Pfennig and Axel Kranzmann, 2018. Degradation of AISI 630 exposed to CO_2-saturated saline aquifer at ambient pressure and 100 bar. Journal of Applied Sciences Research., 14(6): 11-17. DOI: 10.22587/jasr.2018.14.6.3

CO_2 (g) + H_2O (l) → H+ + HCO_3^- (aq) (1)

cathodic: 2 HCO_3^- + 2 e^- → 2 CO_3^{2-} + H_2 (2)

anodic: Fe → Fe^{2+} + 2e^- (3)

Fe^{2+} + CO_3^{2-} → $FeCO_3$ (4)

Fe^{2+} + 2 HCO_3^- → $Fe(HCO_3)_2$ (5)

$Fe(HCO_3)_2$ → $FeCO_3$ + CO_2 + H_2O (6)

The internal and external corrosion layer grow depending on the various carbon and oxygen partial pressures. Local damage of the ferrous hydroxide film due to mechanical and/or chemical effects exposes the highly porous non-protective ferrous carbonate to the geothermal water with lower pH. The ferrous carbonate film begins to dissolve and depassivate the steel. Local surface degradation is enhanced because oxygen vacancies consolidate and condense at the hydroxide/brine interface and detach the siderite from the hydroxide film in lateral direction in direction of the applied mechanical stress. The flowing corrosive media removes the remaining film causing the pit to grow wider, because the same steps will occur from the beginning on the newly exposed surface. Simultaneously crack propagation will take place due to the dynamic load and forces at the pit bottom, because the stress concentrations and plastic deformation lead to the production of slip bands [26] highly susceptible to the corrosion explained. The crack flanks are immediately wetted repeating the corrosion steps within the crack itself.
Results of this paper have been published before [35],[36],[38], but have partly been reconducted (S-N-curve) and are now supported by discussions and summarized findings.

2. MATERIAS AND METHODS

2.1. Surface and Local Corrosion

Static corrosion tests as well as corrosion fatigue tests were carried out using samples of martensitic AISI 630 (1.4542; X5CrNiCuNb16-4)
To simulate in-situ geothermal condition the geothermal aquifer water (as known to be similar to the Stuttgart Aquifer [42]: Ca^{2+}: 1760 mg/L, K^{2+}: 430 mg/L, Mg^{2+}: 1270 mg/L, Na^{2+}: 90,100 mg/L, Cl^-: 143,300 mg/L, SO_4^{2-}: 3600 mg/L, HCO_3^-: 40 mg/L) was synthesized in a strictly orderly way to avoid precipitation of salts and carbonates.
Laboratory scale exposure tests in CO_2-saturated aquifer brine and water saturated CO_2 were carried using coupons of the steel quality AISI 630 may be used as injection pipe using samples made of thermally treated specimen of steels with 8 mm thickness, 20 mm width, 50 mm length. Heat treatment to gain martensitic microstructure with sufficient hardness and toughness prior to exposure was done following commonly used protocols
A hole of 3.9 mm diameter was used for sample positioning. Samples of each base metal were positioned within the vapour phase and within the liquid phase. Flow control (3 NL/h) of the technical CO_2 (purity 99,995 vol.-%)) into the brine at ambient pressure was done by a capillary meter GDX600_man by QCAL Messtechnik GmbH, Munic. The exposure of the samples between 700 h to 8000 h was disposed in reaction vessels according to the conditions at the geological site at 60 °C at ambient pressure – each material in a separated reaction vessel [15], [43] and at 100 bar [44], [45] (Fig. 1).

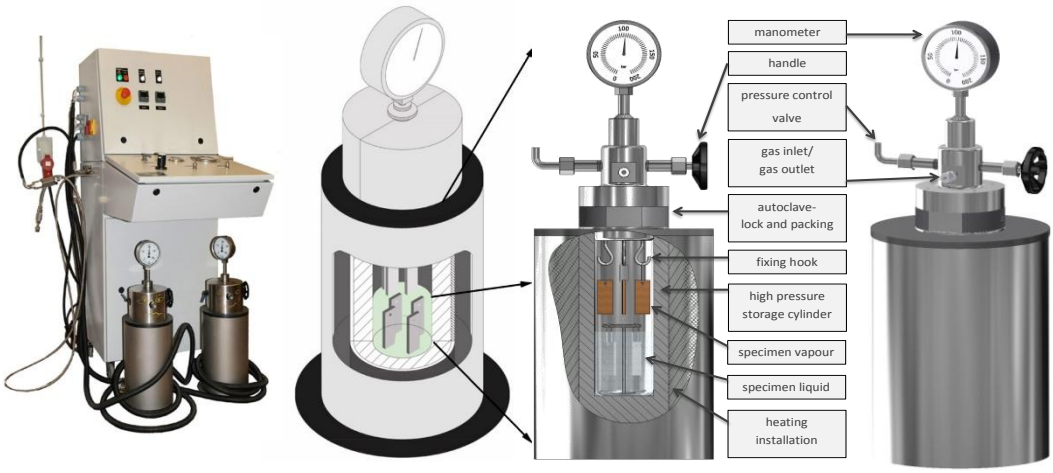

Fig. 1. Reaction vessels and experimental set up [38], [45].

Before corrosion tests the surfaces of the steels were activated by grinding with SiC-Paper down to 120 µm under water. After the corrosion tests, the samples were cut partly for scale analysis with the corrosion layer and prepared partly for kinetic analysis after the scale was etched. Descaling of the samples was performed by exposure to 37% HCl. Then parts of the samples were embedded in a cold resin (Epoxicure, Buehler), cut and polished first with SiC-Paper from 180 µm to 1200 µm under water and then finished with diamond paste 6 µm and 1 µm.

2.2. Corrosion Fatigue

An appropriate system for fatigue testing at temperatures existing in deep geological layers (in-situ conditions) was set up, to assess materials of components loaded cyclically and exposed constantly to the highly corrosive hot thermal water at 60 °C and ca. 20 % salinity of the geothermal water and fluid properties differing strongly [42]. Fatigue tests were carried out using samples of martensitic AISI 630, tensile strength in air: 1078 MPa) (table 1). The surfaces were activated via machining to Rz=4.

The objective was to simulate in-situ conditions (temperature 60 °C, corrosive environment) of a material exposed to dynamic mechanical stress and corrosive gas- saturated saline aquifer environment. The corrosion chamber is fixed directly onto the sample leaving the resonant testing machine unaffected (Fig. 2). During mechanical stress-strain tests a magnetically driven gear pump constantly pumps the corrosive media from the reservoir to the corrosion- and temperature-resistant corrosion chamber. The specimen is during the complete test surrounded of the corrosions medium. Heating is realized by a heating element which is placed at the reservoir. The ratio of sample surface to volume of the corrosive media after DIN 50905 Part 1 (10 ml/cm²) is greater than required. The connecting of the chamber onto the specimen via clamping collar creates a force-fit process ensuring enough force to the corrosion chamber at high frequencies to keep it firmly on the test specimen. The corrosion chamber is sealed by O-rings made of Viton in the area of restraint. In order not to impede the change in length of the sample during the experiment, a membrane is applied to the corrosion chamber as a motion-compensating element.[44], [45].

Citation: Anja Pfennig and Axel Kranzmann, 2018. Degradation of AISI 630 exposed to CO_2-saturated saline aquifer at ambient pressure and 100 bar. Journal of Applied Sciences Research., 14(6): 11-17. DOI: 10.22587/jasr.2018.14.6.3

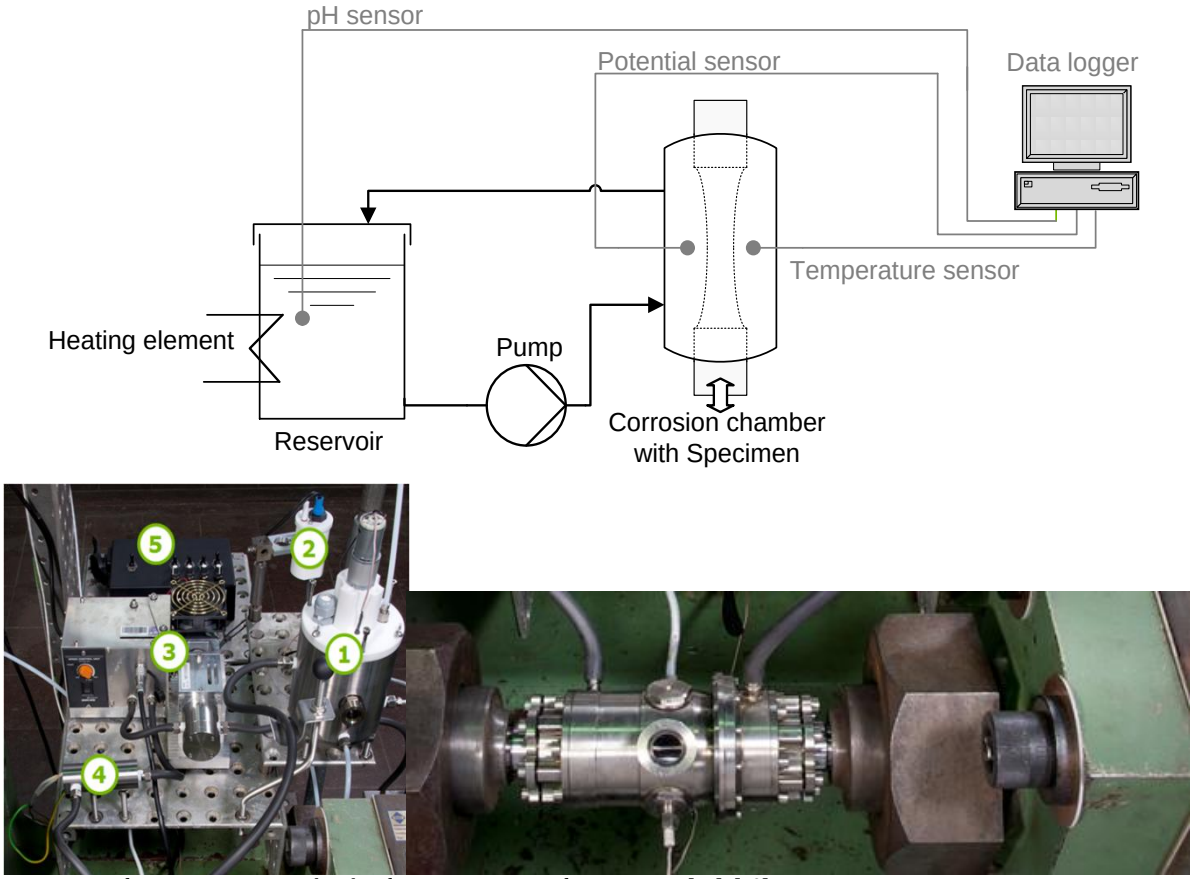

Fig. 2. Schematic set-up of operating corrosion chamber for in-situ corrosion fatigue testing [15], [40].

Electrochemical data were collected in the corrosion chamber during the mechanical tests along with temperature, pH and electrochemical potential. For measurement of the electrochemical potential a shock resistant silver-silver chloride electrode was fixed in a Teflon channel. To simulate non-static operation a resonant testing machine has been used at 30 – 40 Hz where samples of both steels were tested in stress-strain mode under CCS aquifer environment. In addition technical CO_2 was introduced into the closed system at a rate close to 9 L/h to keep stable environmental conditions.

The corrosion fatigue strength of stainless steel with16% chromium AISI 630, hardened and tempered with martensitic microstructure) is examined in dynamic stress-strain tests in CO_2-saturated aquifer (Stuttgart Aquifer [40]) at 60 °C. Therefore a resonant testing machine (sinusoidal dynamic test loads, R=-1; resonant frequency ~ 30 Hz) has been used. In addition technical CO_2 was introduced into the closed corrosion chamber system at a rate close to 9 L/h to keep stable environmental conditions. In each test series 30 specimens were tested. AISI 630 was tested between 150 MPa and 500 MPa. Due to the rather heterogeneous fine machined surfaces (surface roughness Rz=4) the specimens are comparable with prefabricated parts.

Different light optical and electron microscopy techniques were performed on specimens to investigate the layer structures and morphology of the samples. X-ray diffraction was carried out in a URD-6 (Seifert-FPM) with CoKα-radiation with an automatic slit adjustment, step 0.03° and count 5 sec. Phase analysis was performed by matching peak positions automatically with PDF-2 (2005) powder patterns. Mainly structures that were likely to precipitate from the steels were chosen of the ICSD and refined to fit the raw-data-files using POWDERCELL 2.4 [46] and AUTOQUAN ® by Seifert FPM. To characterize the pitting corrosion, 3-D-images were realized by the double optical system Microprof TTV by FRT. Kinetics of the corrosion were determined by the corrosion rates which were calculated via mass change of the samples before and after corrosion testing according to DIN 50 905 part 1-4 and using the semi-automatic analyzing program Analysis Docu ax-4 by Aquinto.

3. STATIC CORROSION

In general the pressure has little to no influence on the corrosion rates regardless of atmosphere (water saturated supercritical CO_2 or CO_2-saturated brine) (Fig. 3). That allows for corrosion tests to be easily conducted at ambient pressure instead of the more time-consuming high pressure test equipment. Maximum corrosion rate in the liquid phase is approximately 0.014 mm/year, after 8000 h and approximately 0.003 mm/year in the supercritical phase.

In agreement with the independence of the corrosion rates on pressure, samples exposed to water saturated supercritical CO_2 and CO_2-saturated brine do not reveal a distinct dependence on the heat treatment prior to exposure showing the same trends during the entire exposure time. [38] The influence on heat treatment prior to exposure has been widely described [11],[22],[28],[29]. Under supercritical CO_2 conditions a martensitic microstructure of hardened and tempered AISI 630 at low temperatures (650 °C) (< 0.001 mm/year) and under saline water normalized microstructure (ca. 0.004 mm/year) offer best corrosion resistance regarding surface corrosion [45].

Citation: Anja Pfennig and Axel Kranzmann, 2018. Degradation of AISI 630 exposed to CO_2-saturated saline aquifer at ambient pressure and 100 bar. Journal of Applied Sciences Research., 14(6): 11-17. DOI: 10.22587/jasr.2018.14.6.3

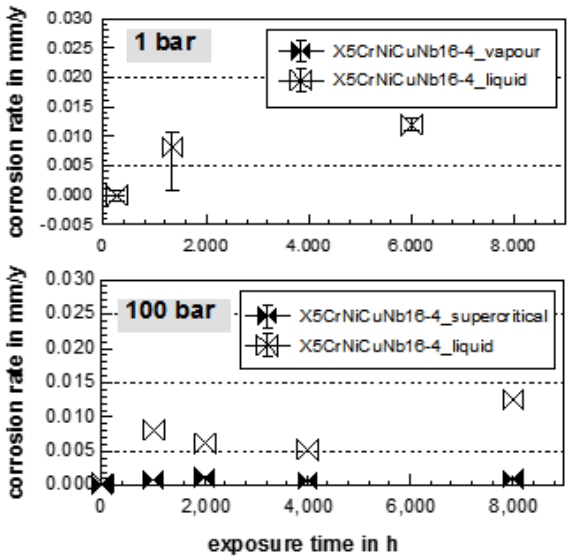

Fig. 3. Corrosion rate of AISI 630 [47] as a function of pressure in water saturated supercritical CO_2 and CO_2 saturated saline aquifer water ([38], [45], [49]) at 60 °C and 100 bar.

AIAI 630 developed a rather high number of pits per m^2 in both atmospheres, water saturated supercritical CO_2 and CO_2 saturated aquifer water (Fig. 4). The number of pits precipitated in the supercritical phase is approximately ten times higher than in the liquid phase. Pit depths measured after exposure at 100 bar and 60 °C are about 10-250 µm.

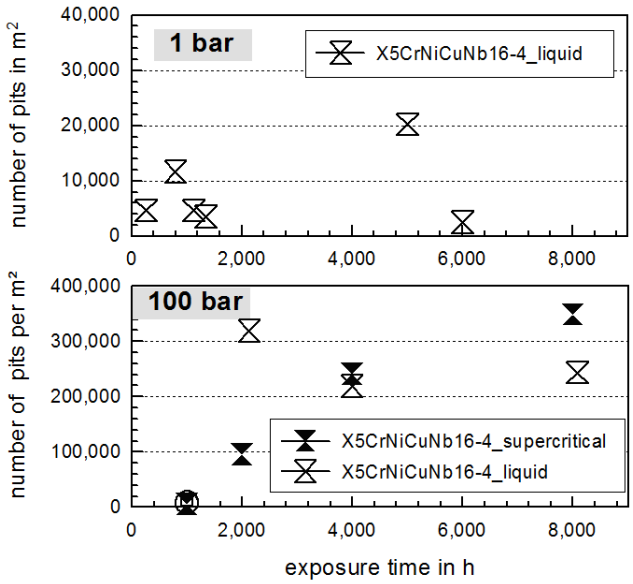

Fig. 4. Number of pits of AISI 630 in the liquid phase after 6000/8000 h of exposure to aquifer brine water at 60 °C and ambient pressure as well as at 100 bar [47].

Corrosion rates obtained in supercritical CO_2 do not change as a function of time. But, long exposure times in CO_2-saturated brine lead to increasing surface corrosion rates after 4000 h due to a possible break-down of the initial passivating layer formed after 1000 h of exposure. Possibly the increasing carbide precipitation depletes the metal matrix of chromium and therefore prohibits further surface passivation. [38], [45].

AISI 630 passivated immediately when exposed to CCS-atmosphere and shows very low corrosion rates in water saturated supercritical CO_2. This depends either on the lack of electrolytes [42] or more possible on the cathodic reaction described in equation (1) leading to a higher H_2CO_3 concentration and therefore more acidic and reactive environment as in the CO_2 saturated liquid phase [7],[26], [38]. In CO_2-containing water carbonic acid is formed due to the low pH and because the solubility of iron carbonate $FeCO_3$ is low [29] siderite forms. This reaction continuous constantly during exposure time leading to the typical leopard shaped corrosion layer consisting of siderite $FeCO_3$ and goethite a-FeOOH as precipitation phases (Fig. 5).

Citation: Anja Pfennig and Axel Kranzmann, 2018. Degradation of AISI 630 exposed to CO_2-saturated saline aquifer at ambient pressure and 100 bar. Journal of Applied Sciences Research., 14(6): 11-17. DOI: 10.22587/jasr.2018.14.6.3

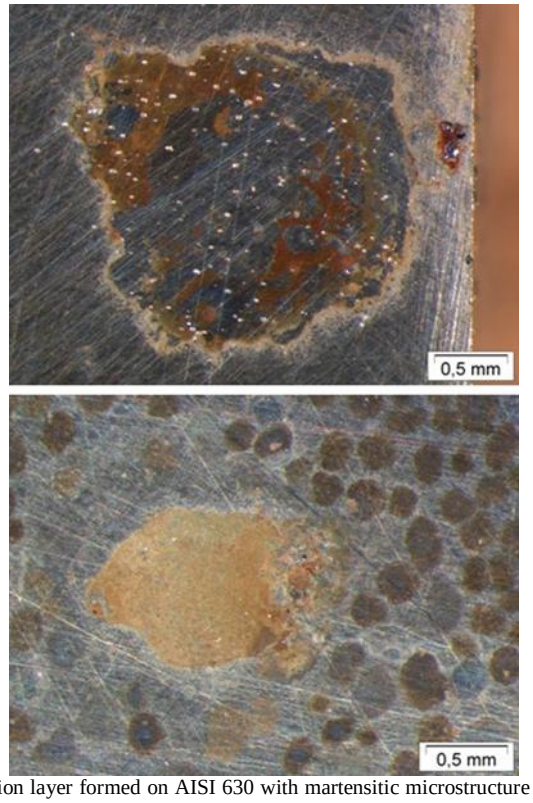

Fig. 5. SEM micrographs of the ellipsoidal corrosion layer formed on AISI 630 with martensitic microstructure prior to exposure after 8000 hours of exposure at 60 °C and 100 bar to water saturated supercritical CO_2 (top) and CO_2-saturated aquifer water (bottom).

The "leopard shape" is subject to further investigation, but it is likely that carbides are more susceptible to corrosion initiation [27], [45], [38] and therefore the passivation of the steel surface is locally destroyed where carbides precipitated. The initiation of this process is limited to the phase boundaries of carbide and surrounding base material. Therefore the pattern reveals spots of different sizes that vary in precipitations: sulphates ($FeSO_4$) in the outer areas whereas the center shows hematite (Fe_2O_3) (Fig. 5). It is also possible that in water saturated supercritical CO_2 at 100 bar and 60 °C the decreasing water solubility in the supercritical carbon dioxide [26] leads to wetting of the metal surface via very thin and small water droplets. Because time was too short to precipitate pits the typical "leopard" shaped corrosion layer is formed indicating the initial droplets on the surface [45]. Areas of former droplets consolidate resulting in small pits surrounding the former droplet (Fig. 4). [38], [45].

4. DYNAMIC IN-SITU CORROSION (HCF)

The corrosion fatigue behaviour was described by Pfennig et al. [38], [44],[45]. In general, the corrosion fatigue strength of AISI 630 is 60% below the endurance limit measured in air (620 MPa) [38], [44], [45] and he decrease of the fatigue limit line with increasing number of cycles (Wöhler-exponent of k = 3.59 in earlier studies [38], [44], [45], now k = 1) is still larger in corrosive environment than in air. [41]. Revised data for the S-N-curve now does not show typical fatigue strength (Fig. 6) as stated before. However, the large scatter range TN=1:34 [44], [45], was now revised with new data, giving a higher reliability of the results. Stress amplitude of 130 MPa gives a maximum number of cycles (1.5×10^6).

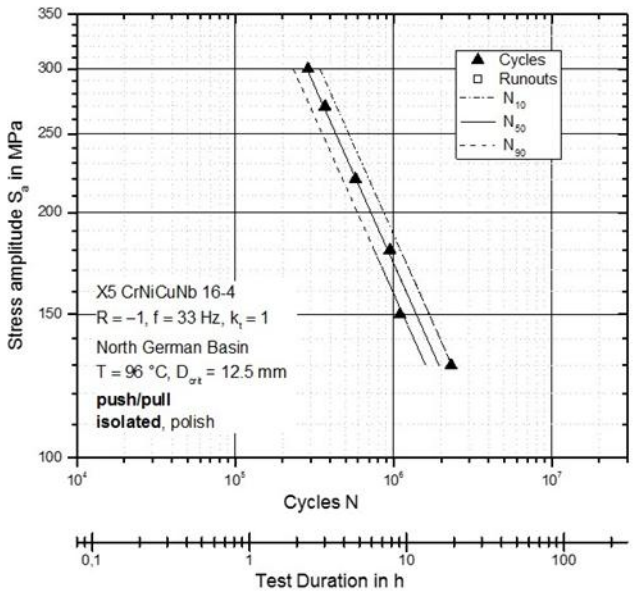

Fig. 6. Revised S-N-curve of AISI 630 exposed to flowing saline aquifer and CO_2 at 60 °C. In agreement with [43], [49], [50] the slope is very steep indicating.

The entire sample area of AISI 630 shows multiple cracks initiated from pits which are most likely responsible for early failure (Fig. 7). The needle type microstructure of AISI 630 (martensitic after hardening and annealing) shows embedded δ-ferrite precipitates. These along with possible discontinuous carbide

Citation: Anja Pfennig and Axel Kranzmann, 2018. Degradation of AISI 630 exposed to CO_2-saturated saline aquifer at ambient pressure and 100 bar. Journal of Applied Sciences Research., 14(6): 11-17. DOI: 10.22587/jasr.2018.14.6.3

distribution may lead to corrosion initiation. However, impurities were found on various surfaces with no significant correlation to the endurance limit). But, samples with low number of cycles to failure contained Al within the corrosion layer and revealed non-metallic inclusions that were ordered discontinuously laterally within the alloy.

Surfaces revealed corrosion layers mainly composed of iron carbonate (siderite, $FeCO_3$) and iron hydroxide ($Fe(OH)_2$). Both, the presence and the thickness of the corrosion layer could not be related to early failure. The number of striations indicating the opening and closing of the initial crack during cyclic load was also not a matter of early or late failure.

The presence of chlorides within the microstructure[51], [52] and increased dislocation number, grain boundaries, boundaries of precipitation phases e.g. carbides leading to local lattice mismatch resulting in higher local boundary energy [50]. Impurities such as Al as well as carbides present in the base material may consolidate during cyclic loading within corrosive environment. The consolidates impurities as well as carbides change lattice energy at the phase boundaries which enhances initial corrosion that then leads to unpredictable early failure.

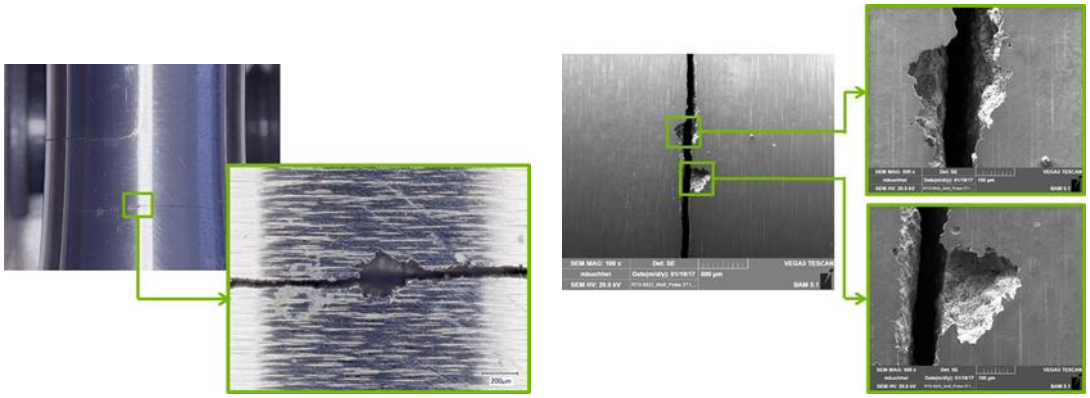

Fig. 7. Crack surfaces after fatigue failure. The crack is accompanied with local corrosion phenomena.

In general, reliable corrosion rates and lifetime predictions regarding pit corrosion and corrosion fatigue for AISI 630 in CCS technology are not possible. Corrosion fatigue in the passive state, that is: crack formation correlated with pit corrosion phenomena, results in inter crystalline corrosion. It is also likely that impurities lead to local corrosion phenomena that then enhance crack initiation. Al is the only significant evidence for possible lower endurance limits. But again failure is not necessary a consequence of local corrosion. These findings still do not fully explain the unusual corrosion and corrosion fatigue behavior of the metal and are therefore subject to further research.

5. CONCLUSION

Surface corrosion rates of AISI 630 are lower in supercritical CO_2, but pit corrosion resistance is better in CO_2 saturated brine. The “leopard structured” surface corrosion is related to the change in microstructure and environmental conditions, such as: chemical decomposition, water and CO_2 partial pressure, presence of electrolyte, pH and early pit formation. $FeCO_3$ and FeOOH are corrosion products under static and dynamic corrosion tests as well as in surface corrosion layers as in pits. Despite the surface degradation usually causing crack initiation no correlation could be found for inclusions and early rupture. However, specimens with inclusions at the fracture surface and its cross section endured lower number of cycles and Al was analyzed in specimens with low number of cycles and may be cause for early rupture during corrosion fatigue tests.

Corrosion rates, local corrosion accompanied with crack initiation are decisive when deciding if the steels are suitable for CCS application. Steels will be unsuitable for its use in pressure vessel applications if the corrosion rate exceeds 0,1 mm/year. A high sensitivity on a homogeneous microstructure upon the corrosion and corrosion fatigue behaviour of AISI 630 needs to be taken into account when regarding this steel as pipe steel during injection of CO_2 into saline aquifers.

6. ACKNOWLEDGEMENTS

This work was supported by the FNK (Fachkonferenz für wissenschaftliche Nachwuchskräfte) of the Applied University of Berlin, HTW and by IMPACT (EU-Project EFRE 20072013 2/21).

7. REFERENCES

[1] D.C. Thomas, 2005. Carbon Dioxide Capture for Storage in Deep Geologic Formations - Results from CO_2 Capture Project, Volume 1: Capture and Separation of Carbon Dioxide form Combustion Sources, CO_2 Capture Project, Elsevier Ltd UK ISBN 0080445748

[2] M. van den Broek, R. Hoefnagels, E. Rubin, W. Turkenburg, A. Faaij, 2010. Effects of technological learning on future cost and performance of power plants with CO_2 capture, in Projects Costs of Generating Electricity, Progress in Energy and Combustion Science, 177-187, ISBN 978-92-64-08430-8

[3] S. Nešic, 2007. Key issues related to modelling of internal corrosion of oil and gas pipelines - A review", Corrosion Science 49 :4308-4338

[4] S. Hurter, Impact of Mutual Solubility of H_2O and CO_2 on Injection Operations for Geological Storage of CO_2, International Conference of the Properties of Water and Steem ICPWS, Berlin, September 8-11

[5] L. Zhang, J. Yang, J.S. Sun, M. Lu, 2008. Effect of pressure on wet H_2S/CO_2 corrosion of pipeline steel, No. 09565, NACE Corrosion 2008 Conference and Expo, New Orleans, Louisiana, USA, March 16th - 20th,

[6] L.J. Mu, W.Z. Zhao, 2009. Investigation on Carbon Dioxide Corrosion Behaviors of 13Cr Stainless Steel in Simulated Strum Water, Corrosion Science, Manuscript No. CORSCI-D-09-00353 1-24

[7] M. Seiersten, 2001. Material selection for separation, transportation and disposal of CO_2, NACE Corrosion, Corrosion paper no. 01042

[8] Z.D. Cui, S.L. Wu, S.L. Zhu, X.J. Yang, 2006. Study on corrosion properties of pipelines in simulated produced water saturated with supercritical CO2, Applied Surface Science 252:2368-2374

[9] Pfennig, A., Kranzmann, A, 2011. Reliability of pipe steels with different amounts of C and Cr during onshore carbon dioxide injection, International Journal of Greenhouse Gas Control 5:757-769

[10] H. Zhang, Y.L Zhao, Z.D. Jiang, 2005. Effects of temperature on the corrosion behaviour of 13Cr martensitic stainless steel during exposure to CO2 and Cl-environment, Material Letters 59:3370-3374

[11] J.N. Alhajji and M.R. Reda, 1993. The effect of alloying elements on the electrochemical corrosion of low residual carbon steels instagnant CO_2-saturated brine, Corrosion Science, 34(11):1899-1911

[12] Y.-S. Choi, S. Nešic, 2008. Corrosion behaviour of carbon steel in supercritical CO_2-water environments, No. 09256, NACE Corrosion 2008 Conference and Expo, New Orleans, Louisiana, USA.

[13] X. Jiang, S. Nešic, F. Huet, 2008. The Effect of Electrode Size on Electrochemical Noise Measurements and the Role of Chloride on Localized CO_2 Corrosion of Mild Steel, Paper No. 09575, NACE Corrosion 2008 Conference and Expo, New Orleans, Louisiana, USA.

Citation: Anja Pfennig and Axel Kranzmann, 2018. Degradation of AISI 630 exposed to CO_2-saturated saline aquifer at ambient pressure and 100 bar. Journal of Applied Sciences Research., 14(6): 11-17. DOI: 10.22587/jasr.2018.14.6.3

[14] Z. Ahmad, I.M. Allam, B.J. Abdul Aleem, 2000. Effect of environmental factors on the atmospheric corrosion of mild steel in aggressive sea coastal environment, Anti Corrosion Methods and Materials, 47:215-225
[15] Pfennig, R. Bäßler, 2009. Effect of CO_2 on the stability of steels with 1% and 13% Cr in saline water, Corrosion Science, 51(4):931-940,
[16] Pfennig, A. Kranzmann, 2010. The role of pit corrosion in engineering the carbon storage site Ketzin, Germany, WIT Transactions on Ecology and the Environment, Volume 126:109-118, ISBN: 978-1-84564-450-5
[17] A. Pfennig, P. Zastrow, A, 2013. Kranzmann, Influence of heat treatment on the corrosion behaviour of stainless steels during CO2-sequestration into saline aquifer, International Journal of Green House Gas Control 15:213-224
[18] R. Nyborg, 2005. Controlling Internal Corrosion in Oil and Gas Pipelines, Business Briefing: Exploration & Production: The Oil & Gas Review, 2:70-74
[19] D.S. Carvalho, C.J.B. Joia, O.R. Mattos, 2005. Corrosion rate of iron and iron-chromium alloys in CO2-medium, Corrosion Science 47:2974-2986
[20] B.R. Linter, G.T Burstein, 1999. Reactions of pipeline steels in carbon dioxide solutions, Corrosion Science 41:117-139
[21] S.L Wu, Z.D. Cui, G.X. Zhao, M.L. Yan, S.L. Zhu, X.J. Yang, 2004. EIS study of the surface film on the surface of carbon steel form supercritical carbon dioxide corrosion", Applied Surface Science 228:17-25
[22] S. Bülbül, Y Sun, 2010. Corrosion behaviours of high Cr-Ni cast steels in the HCl solution, Journal of Alloys and Compounds 598:143-147
[23] Hou, Y. Li, Y. Li, J. 2000. Zhang, Effect of alloy elements on the anti-corrosion properties of low alloy steel, Bull. Mater. Sci, 23(3):189-192
[24] Z. Cvijovic and G. Radenkovic, 2006. Microstructure and pitting corrosion resistance of annealed duplex stainless stell, Corrosion Science 48:3887-3906
[25] J.-Y. Park, Y.-S. Park, 2007. The effects of heat-treatment parameters on corrosion resistance and phase transformation of 14Cr-3Mo martensitic stainless steel, Materials Science and Engineering A 449-451 1131-1134
[26] J. Banas, U. Lelek-Borkowska, B. Mazurkiewicz, W. Solarski, 2007. Effect of CO_2 and H_2S on the composition and stability of passive film on iron alloy in geothermal water, Electrochimica Acta 52:5704-5714
[27] P.D. Bilmes, C.L. Llorente, C.M. Méndez, C.A. Gervasi, 2009. Microstructure, heat treatment and pitting corrosion of 13CrNiMo plate and weld metals, Corrosion Science, ISSN: 0010-938X, Vol: 51, Issue: 4:876-882
[28] L. Zhang, W. Zhang, Y. Jiang, B. Deng, D. Sun, J. Li, Influence of annealing treatment on the corrosion resistance of lean duplex stainless steel 2101
[29] Brown, S. R. Parakala, S. Nešic, 2004. CO_2 corrosion in the presence of trace amounts of H_2S, Corrosion, paper no. 04736:1-28
[30] N. Isfahany, H. Saghafian, G. Borhani, 2011**.** The effect of heat treatment on mechanical properties and corrosion behaviour of AISI420 martensitic stainless steel, Journal of Alloys and Compounds 509:3931-3936
[31] M.A. Lucio-Garciaa, J.G. Gonzalez-Rodrigueza, , M. Casalesc, L. Martinezc, J.G. Chacon-Navaa, M.A. Neri-Floresa and A. Martinez-Villafañea, 2009. Effect of heat treatment on H_2S corrosion of a micro-alloyed C-Mn steel, Corrosion Science 51:2380-2386
[32] Madduri and R. V. Prakash, 2010. Corrosion Fatigue Crack Growth Studies in Ni-Cr-Mn steels, International Journal of Mechanical and Materials Engineering 1:20-25.
[33] M. Seo, 1999. Electrochemical Society. Corrosion Division, Passivity and localized corrosion: an International Symposium in Honour of Professor Norio Sato, initiation and stability of localized corrosion processes on stein steels, 483-490, The Electrochemical Society,
[34] V. Vignal, O. Delrue, J. Peultier, R. Oltra, 2007.. Critical Factors in Localized Corrosion 5: A Symposium in Honour of Hugh Isaacs, Local mechanical-electrochemical behavior of duplex stainless steels, 102-104, The Electrochemical Society,
[35] Pfennig, M. Wolf, Th. Böllinghaus, 2016. Corrosion Fatigue of X46Cr13 in CCS Environment, in Energy Technology 2016: Carbon Dioxide Management and Other Technologies 1:49-56
[36] Pfennig, R. Wiegand, M. Wolf, C.-P. Bork, 2013. Corrosion and corrosion fatigue of AISI 420C (X46Cr13) at 60 °C in CO_2-saturated artificial geothermal brine, Corrosion Science 68:134-143
[37] J. Han, Y. Yang, S. Nešic, B. N. Brown, 2008. Roles of passivation and galvanic effects in localized CO2 corrosion of mild steel, Paper No. 08332, NACE Corrosion 2008, New Orleans, Louisiana, USA.
[38] Pfennig, A. Kranzmann, 2017. Potential of martensitic stainless steel X5CrNiCuNb 16-4 as pipe steel in corrosive CCS environment, IJSSD International Journal of Environmental Science and Development. 8(7):466-473
[39] Pfennig, A. Kranzmann, 2018. Effect of CO_2, atmosphere and pressure on the stability of X35CrMo17 stainless steel in laboratory CCS-environment, 14th International Conference on Greenhouse Gas Control Technologies, GHGT-14, Melbourne, Australia
[40] Pfennig, A. Gröber, R. Simkin, A. Kranzmann, 2018. The role of surface texture on the corrosion behavior of high alloyed steels exposed to different saline aquifer water environments, 14th International Conference on Greenhouse Gas Control Technologies, GHGT-14, 21-25. Melbourne, Australia
[41] Pfennig, H. Wolthusen, P. Zastrow, A. Kranzmann, 2015. Evaluation of heat treatment performance of potential pipe steels in CCS-environment, Carbon Dioxide Management and Other Technologies 1:15-22
[42] Förster, B. Norden, K. Zinck-Jørgensen, P. Frykman, J. Kulenkampff, E. Spangenberg, J. Erzinger, M. Zimmer, J. Kopp, G. Borm, C. Juhlin, C. Cosma, S. Hurter, 2006, Baseline characterization of the CO2SINK geological storage site at Ketzin, Germany: Environmental Geosciences, V. 13, No. 3 (September 2006), pp. 145-161.
[43] M. Wolf, R. Afanasiev, T. Böllinghaus, A. 2017. Pfennig, Investigation of Corrosion Fatigue of Duplex Steel X2CrNiMoN22 5 3 Exposed to a Geothermal Environment under Different Electrochemical Conditions and Load Types, Energy Procedia, 114:5337-5345
[44] Pfennig, K. Heynert, M. Wolf, T. Böllinghaus, 2014. First in-situ Electrochemical Measurement During Fatigue Testing of Injection Pipe Steels to Determine the Reliability of a Saline Aquifer Water CCS-site in the Northern German Basin, Energy Procedia, 63:5773-5786
[45] Pfennig, H. Wolthusen, A. Kranzmann, 2017. Unusual corrosion behavior of AISI 630 exposed a laboratory saline aquifer water CCS-environment, Energy Procedia, 114:5229-5240
[46] SW. Kraus and G. Nolze, 1996. POWDER CELL - a program for the representation and manipulation of crystal structures and calculation of the resulting X-ray powder patterns, J. Appl. Cryst. 29:301-303
[47] Pfennig, A. Kranzmann, 2018. Impact of saline aquifer water on surface and shallow pit corrosion of martensitic stainless steels during exposure to CO_2 environment (CCS), International Conference on Future Environment and Energy ICFEE 2018.
[48] Pfennig, A. Kranzmann, 2018. Impact of saline aquifer water on local corrosion of martensitic stainless steels during exposure to CO_2 environment (CCS), International Conference on Future Environment and Energy ICFEE 2018.
[49] Pfennig, H. Wolthusen, M. Wolf, A. Kranzmann, 2014. Effect of heat treatment of injection pipe steels on the reliability of a saline aquifer water CCS-site in the Northern German Basin, Energy Procedia, 63:5762-5772
[50] Pfennig, M. Wolf, A. Gröber, T. Böllinghaus, A. Kranzmann, 2017. Corrosion fatigue of AISI 630 exposed to a laboratory saline aquifer water CCS-environment, Energy Procedia, 114:5219–5228
[51] Unigovski, Ya.B., Lothongkum, G., Gutman, E.M., Alush, D., Cohen, R., 2009. Low-cycle fatigue behaviour of 316L-type stainless steel in chloride solutions, Corrosion Science. 51:3014-3120.
[52] Pfennig, A., Wiegand, R., Wolf, M., Bork, C.-P., 2013. Corrosion and corrosion fatigue of AISI 420C (X46Cr13) at 60 °C in CO_2-saturated artificial geothermal brine, Corrosion Science 68:s134-143